AGU PUBLICATIONS

Journal of Advances in Modeling Earth Systems

RESEARCH ARTICLE

10.1002/2016MS000674

Key Points:
- Assimilating MWHS with 3DVAR improves wind, temperature, and humidity
- The Hybrid experiment further improves the track, intensity, and precipitation forecast
- It is more appreciable to apply the Hybrid for Linfa

Correspondence to:
D. Xu,
xdmjolly@sina.com

Citation:
Xu, D., J. Min, F. Shen, J. Ban, and P. Chen (2016), Assimilation of MWHS radiance data from the FY-3B satellite with the WRF Hybrid-3DVAR system for the forecasting of binary typhoons, *J. Adv. Model. Earth Syst.*, *8*, 1014–1028, doi:10.1002/2016MS000674.

Received 27 MAR 2016
Accepted 22 MAY 2016
Accepted article online 27 MAY 2016
Published online 25 JUN 2016

Assimilation of MWHS radiance data from the FY-3B satellite with the WRF Hybrid-3DVAR system for the forecasting of binary typhoons

Dongmei Xu[1], Jinzhong Min[1], Feifei Shen[1], Junmei Ban[2], and Peng Chen[3]

[1]Key Laboratory of Meteorological Disaster, Ministry of Education (KLME)/Joint International Research Laboratory of Climate and Environment Change (ILCEC)/Collaborative Innovation Center on Forecast and Evaluation of Meteorological Disasters (CIC-FEMD), Nanjing University of Information Science & Technology, Nanjing, China, [2]National Center for Atmospheric Research, Boulder, Colorado, USA, [3]Jiangsu Meteorological Information Center, Nanjing, China

Abstract Chan-hom and Linfa were binary typhoons that occurred in the western North Pacific in 2015. In this study, the impacts of FY-3B satellite Microwave Humidity Sounder (MWHS) radiance observations on the analyses and forecasts of Linfa and Chan-hom are assessed. The regional Weather Research and Forecasting model and its data assimilation (DA) systems, using three-dimensional variational (3DVAR) and Hybrid (ensemble/3DVAR) methods are used. Assimilation of the FY-3B MWHS data using the 3DVAR method slightly improves the descriptive wind and temperature fields. Positive impacts on the specific humidity forecasts, for levels higher than 850 hPa, are also obvious. 3DVAR adjusts the typhoons' initial positions and their dynamic structures favorably, yielding better tracks, intensities, and precipitation forecasts, compared to the experiment run without MWHS data (control). With the Hybrid method, the water vapor information from the MWHS data better improve the analyses through multivariable correlations with the flow-dependent background error. The Hybrid method further improves the track, intensities, and precipitation forecasts. For Typhoon Linfa, with the coexistence of Typhoon Chan-hom, the Hybrid method provides a more descriptive background error covariance matrix, than using 3DVAR. Experiments on multiple binary typhoon cases are also provided to further validate the robustness of the results on the FY-3B satellite MWHS radiance data assimilation.

1. Introduction

The predictability of the tracks and intensities of binary tropical cyclones (TCs), which are present simultaneously in the same region, are relatively low, due to the interactions between the TCs. Advancements in data assimilation (DA) techniques during the initialization of TCs, and the assimilation of more observations, have contributed to large reductions in the error of TC track and intensity forecasts [e.g., *Li and Liu*, 2009; *Schwartz et al*., 2012; *Liu et al*., 2012; *Xu et al*., 2013; *Shen et al*., 2015; *Xu et al*., 2015]. Improving predictions of rainfall amounts and distributions during TCs provides another challenging task for the TC research [*Yen et al*., 2011; *Schwartz and Liu*, 2014]. Satellite observations play a very important role in improving the accuracy of numerical weather prediction, especially over areas with sparse conventional observations [e.g., *McNally et al*., 2000; *Zapotocny et al*., 2008; *Xu et al*., 2013]; thus, the satellite observation is the key for improving TC forecasts. Recently, microwave satellite observations have contributed the most to improving numerical weather forecasts; the observations have been (or are being) ingested into DA systems [e.g., *Smith et al*., 1979; *Goodrum et al*., 1999; *Li and Liu*, 2009; *Liu et al*., 2012; *Schwartz et al*., 2012; *Newman et al*., 2015; *Shen et al*., 2015]. Examples include the Suomi National Polar-orbiting Partnership (NPP)-Advanced Technology Microwave Sounder (ATMS) data, used in the European Centre for Medium-Range Weather Forecasts (ECMWF) and the National Centers for Environmental Prediction (NCEP) systems (NIELS) [*Niels et al*., 2012; *Collard et al*., 2012]; the NOAA-18 and MetOp-A Microwave Humidity Sounders (MHSs), used in the Weather Research and Forecasting DA system (WRFDA) [*Schwartz et al*., 2012; *Newman et al*., 2015] as well as most operational centers [*Thépaut*, 2003]; and the FY-3A and FY-3B MWHSs, used in the ECMWF system, which is the first operational use of Chinese polar orbiter satellite data by an NWP center outside China [*Lu et al*., 2011ba; *Chen et al*., 2015].Notably, the MHS and MWHS are designed to retrieve profiles of atmospheric water vapor. Atmospheric moisture profiles have been shown to impact tropical convection and cyclones

[*Holloway and Neelin*, 2009]. Compared to the MHSs onboard the MetOp series of satellites, the MWHSs on the FY-3A/B satellites have larger instrument noise [*Zou et al*., 2011; *Chen et al*., 2015].

Among the FY series of polar orbit satellites, FY-3B is the latest one in service [*Lu et al*., 2011b, *Chen et al*., 2015]; the FY-3 series of satellites began with the launch of FY-3A in May 2008 and FY-3B in November 2010 [*Guan et al*., 2011]. The MWHSs provide vertical water vapor data, which are important for numerical weather predictions. Assimilation of MWHS radiance data into the ECMWF Integrated Forecasting System (IFS) was verified to slightly improve the longer-range forecast scores and improved the short-range forecasts, when compared to other observations. ECMWF has been assimilating the FY-3B MWHS observations into its operational forecasting system since September 24, 2014. MWHS radiance observations were found to improve the global and regional operational forecast skills, even with the relatively large MWHS instrument noise [*Lu et al*., 2011a, 2011b; *Chen et al*., 2015]. However, very few studies have directly explored the ability of MWHS radiance data to improve TC forecasts with limited area models and DA systems.

In this study, the WRFDA system is used [*Barker et al*., 2012, *Dong et al*., 2013] for better comparisons with *Newman et al*., 2015, to evaluate the impact of the FY-3B MWHS radiance data on TC forecasting. Besides the three-dimensional variational DA (3DVAR) method, we also apply a Hybrid (ensemble/3DVAR) method to provide a more descriptive background error covariance (BEC); this is because of the relatively low predictability of track and intensity for binary TCs. A binary TC case over the Northwestern Pacific in the summer of 2015 is detailed, which caused severe damage in China. Total six typhoons are selected to achieve solid results. A brief introduction to the WRFDA system and the radiance assimilation methods are provided in section 2. Section 3 describes typhoons "Chan-hom" and "Linfa" (2015). The experimental settings are specified in section 4. Results and conclusions are presented in sections 5 and 6, respectively.

2. Assimilation of FY-3B MWHS Radiances With WRFDA

The data assimilation system WRFDA was developed with 3DVAR, four-dimensional variational DA (4DVAR), and Hybrid (incorporating ensemble-produced background error in the variational framework) DA techniques at the National Center for Atmospheric Research (NCAR) [*Barker et al*., 2012]. The WRFDA system is capable of utilizing a large variety of observations, including satellite radiance data, and can perform data thinning, quality control (QC), and bias corrections. The 3DVAR and Hybrid component of the WRFDA are used in this study. The 3DVAR method aims to obtain a statistically optimal analysis through an iterative minimization of a prescribed cost function (***J*(x)**) [*Ide et al*., 1997; *Wang* 2011]:

$$J(\mathbf{x},\alpha)=\frac{1}{2}\beta_1(\mathbf{x}-\mathbf{x}_b)^T\mathbf{B}^{-1}(\mathbf{x}-\mathbf{x}_b)+\frac{1}{2}\beta_2(\alpha)^T\mathbf{A}^{-1}(\alpha)+\frac{1}{2}(\mathbf{y}-H(\mathbf{x}))^T\mathbf{R}^{-1}(\mathbf{y}-H(\mathbf{x})), \quad ((1),)$$

where "**x**" is the atmospheric state vector for the analysis, "$\mathbf{x}_b$" is the background, "α" is the extra control variable, and "**y**" is the observation vector. "*H*" is the observation operator that maps the model variables to the observation space, while "**B**" and "**R**" are the background and observation error covariance matrices, respectively. The BEC matrix **B** is obtained using control variables [CV option 5 (CV5)] as stream function, the unbalanced part of velocity potential, the unbalanced part of temperature, the unbalanced part of surface pressure Psu, and pseudorelative humidity RH. The term ''unbalanced'' refers to the residual from the balance with the stream function. The pseudorelative humidity is water vapor mixing ratio divided by the saturated specific humidity from the background field. The case-dependent B matrixes are estimated with the National Meteorological Center (NMC) method [*Parrish and Derber*, 1992] by using the differences in the 24 and 12 h forecasts initiated from Global Forecast System (GFS) analyses at 0000 and 1200 UTC for each day of the previous month of the cases for study. "A" is a block diagonal matrix that controls the spatial correlation of "α." The weights of the static and flow-dependent covariances are determined by the factors "β_1" and "β_2." In this study, 50% weights are used for both the static and ensemble-based covariances. The solution of "**x**" represents the estimate of the true atmospheric state by minimizing (1) iteratively [*Lorenc*, 1986]. Details of the schematic of the WRFDA system can be found in *Xu et al*. [2015] and *Shen and Min* [2015].

To assimilate the radiance data, the Community Radiative Transfer Model (CRTM) [*Han et al*., 2006; *Liu and Weng*, 2006] is applied as the forward operator, to compute the clear-sky radiance using the temperature and moisture model profiles. In addition to the forward model, the corresponding tangent linear model, adjoint model, and K-matrix model for computing Jacobians have also been included in the CRTM package.

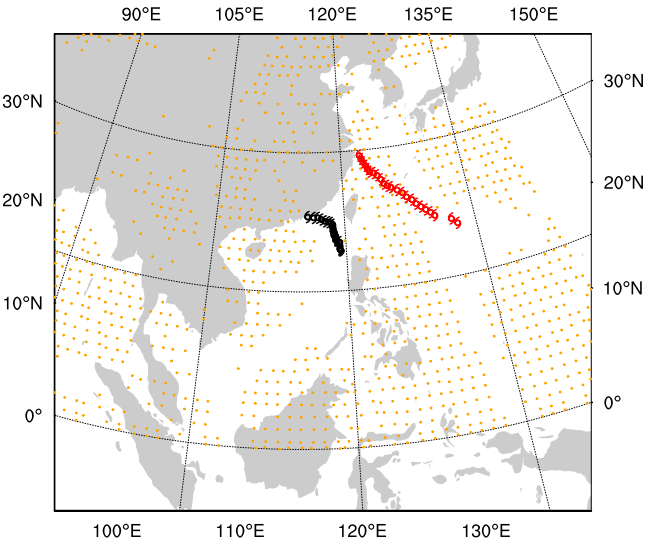

Figure 1. The model domain and the 3 hourly tracks of Linfa (black symbols; from 0600 UTC 8 July to 0600 UTC 11 July 2015) and Chan-hom (red symbols; from 0600 UTC 6 July to 0600 UTC 9 July 2015). The FY-3B MWHS radiance observations available during the assimilation window also shown, as valid at 0600 UTC 8 July 2015 and 0600 UTC 10 July 2015.

Radiances are prone to systematic biases, which need to be corrected before assimilation [*Dee and Uppala*, 2009]. The observation operator is modified to include the bias corrections with a constant component of total bias, as well as seven potentially state-dependent predictors (the scan position, the square, and cube of scan position, 1000–300 hPa and 200–50 hPa layer thicknesses, surface skin temperature, and total column water vapor) and their coefficients. This modified observation operator is widely applied in many studies with limited domain areas [*Liu et al*., 2012; *Schwartz et al*., 2012; *Xu et al*., 2013]. The channel dependent coefficients [*Eyre*, 1992] can be updated by including them as control variables within a variational minimization procedure [*Derber and Wu*, 1998; *Dee and Uppala*, 2009], or can be estimated offline [*Harris and Kelly*, 2001]. The variational bias correction (VarBC) [*Auligné et al*., 2007] scheme is utilized in this study.

3. Overview of Typhoon Cases

This study selected two binary typhoons, Linfa and Chan-hom (2015), to explore the impact of the FY-3B MWHS radiances on typical TCs in the Pacific. The two typhoons both brought heavy rainfall throughout the east of China for several days. Based on the estimate from the Joint Typhoon Warning Center (JTWC), Chan-hom was the strongest typhoon to impact Shanghai in the last 35 years, passing within 160 km. Economic losses from the storm caused by Linfa reached 213 million dollars and 1.46 billion dollars of economic losses were caused by Chan-hom. The main tracks for both events before landfall are shown in Figure 1.

Early on 30 June at 0000 UTC, the Japan Meteorological Agency (JMA) classified a low-pressure system as a tropical depression, located about 345 km northeast of Pohnpei (https://en.wikipedia.org/wiki/Typhoon_Chan-hom_(2015)). The JMA upgraded the cyclone to a tropical storm. Chan-hom then moved steadily to the west. On 3 July, the system turned northeast. Later that day, the broad circulation turned north-northwest. On the next day, Chan-hom skirted the southern coast of Rota, in the Mariana Islands. On 7 July, the typhoon entered the Philippines area of responsibility. The typhoon soon re-established and slowly contracted to a 40 km diameter by 8 July. Late on 9 July, the typhoon passed between the Okinawa and Miyako-jima islands, Japan. Chan-hom reached its peak strength, with estimated winds of 165 km h^{-1} and a barometric pressure of 935 hPa, before making landfall in Zhoushan, Zhejiang around 0840 UTC on 11 July.

In the same period as Chan-hom's early development, Linfa originated from a weak tropical disturbance over the Philippine Sea on June 30. The disturbance gradually intensified and the JMA upgraded the depression to a tropical storm on 1 July. On 3 July, Linfa intensified into a severe tropical storm. By late 4 July, Linfa made landfall over Palanan, Isabela, in the Philippines. The system was downgraded to a tropical storm by JMA several hours later, when it entered the South China Sea. By 6 July, Linfa had moved slowly and maintained its intensity; it was located a few miles west of Taiwan, in a northerly projection. Linfa reached a secondary peak on 8 July as a Category 1 typhoon at this point. Linfa maintained its intensity, at severe tropical storm strength, with a lowest minimum pressure of 975 hPa, and made final landfall in Guangdong, China, on 9 July, two days earlier than Chan-hom.

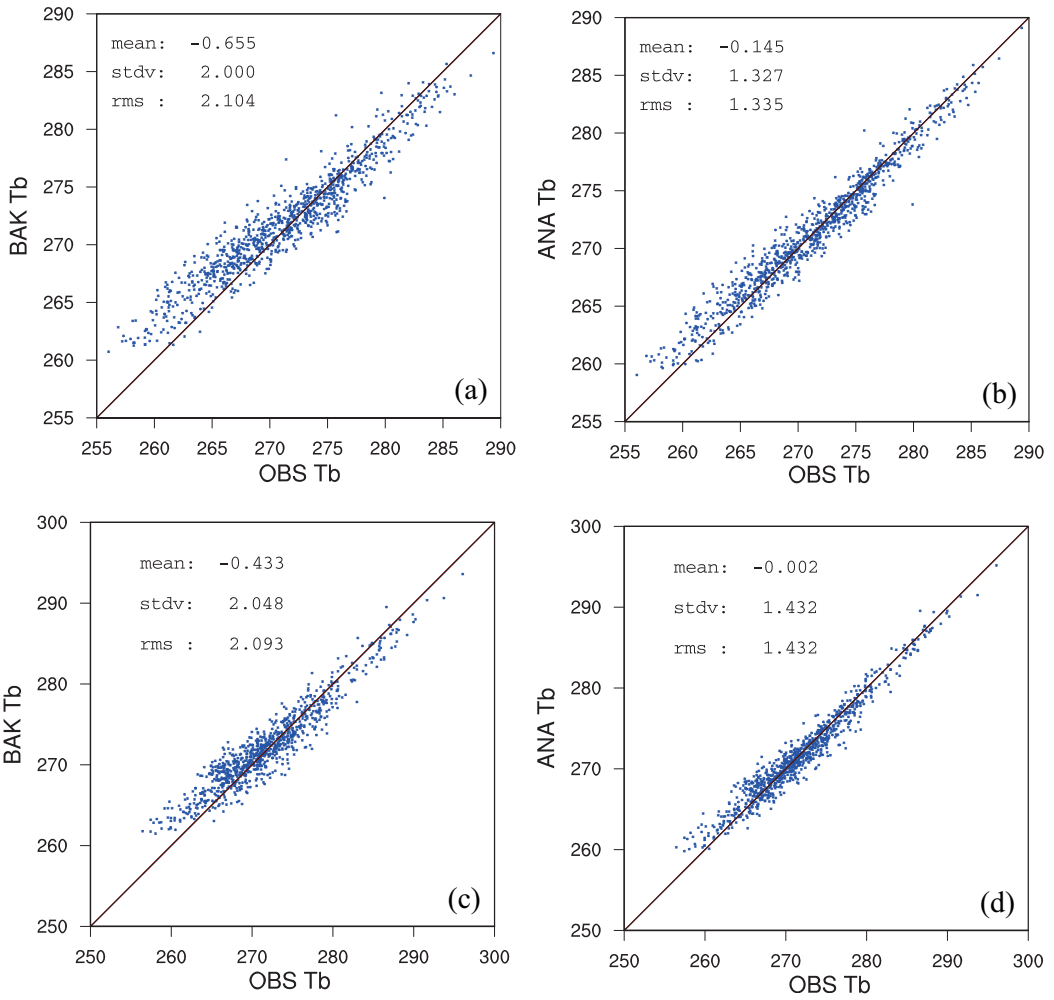

Figure 2. Scatterplots of the observed radiance versus the CRTM-calculated brightness temperature (Tb; K) valid at (a, b) 0600 UTC on 8 July 2015 and (c, d) 0600 UTC on 10 July, 2015; the CRTM-calculated Tb data are from Figures 2a and 2c the background data from channel 5 (wavelength around 13.774 μm) of the FY-3B MWHS; and (b, d) the analysis that uses the 3DVAR method.

4. Experimental Configurations

The model domain applied for the experiments (Figure 1) has a 450 × 400 horizontal grid and 43 vertical levels; the model top is at 30 hPa and the grid spacing is 15 km. Four experiments, denoted as CTRL-3DVar, MWHS-3DVar, CTRL-Hybrid, and MWHS-Hybrid, are conducted for both cases, to evaluate the impact of MWHS radiance data, using the different assimilation methods, on the analyses and subsequent forecasts. The CTRL-3DVar and CTRL-Hybrid experiments assimilate the conventional observations from the NCEP operational Global Telecommunication System (GTS) data set. The MWHS-3DVar experiment assimilates all observations in the "CTRL-3DVar," plus the MWHS radiance data from the FY-3B satellite, using the 3DVAR method. The MWHS-Hybrid experiment is similar to the MWHS-3DVar experiment with the same set of conventional and radiance observations, but uses the Hybrid method instead of the 3DVAR method.

For Chan-hom, the data assimilation is valid at 0600 UTC on 10 July 2015. The background for the analysis is the forecast initiated from the NCEP operational GFS 0.5° × 0.5° analysis at 0000 UTC on 10 July 2015. The lateral boundaries for the forecasts are provided by the GFS analyses at 6 h time intervals. Similar DA and forecast configurations are used for Linfa; the analysis time is valid at 0600 UTC on 8 July 2015, with the 6 h forecast initialized from the GFS analysis at 0000 UTC on 8 July 2015, as the background. It is worth pointing out that the existence of Typhoon Chan-hom makes the simulation and prediction of Linfa more challenging at 0600 UTC on 8 July 2015.

In these experiments, MWHS radiance data are assimilated with the appropriate quality control (QC), channel selection, and bias corrections. Only channels 3, 4, and 5 are assimilated, which correspond to the

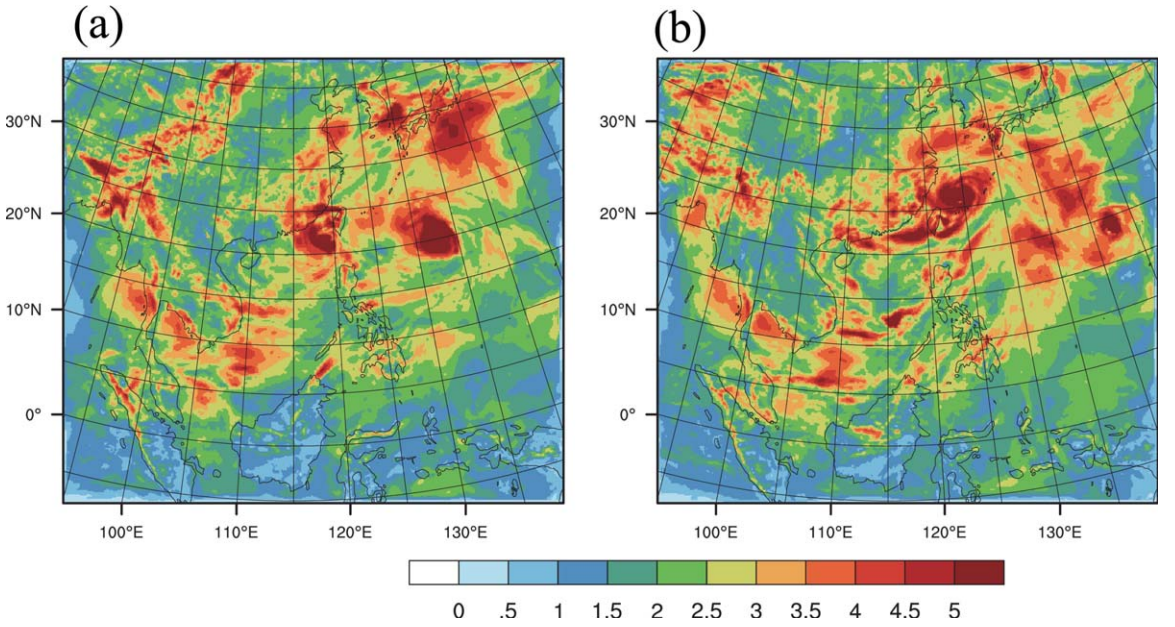

Figure 3. Ensemble spread of wind speed (m s^{-1}) at the seventh model level, valid at (a) 0600 UTC 8 July 2015, and (b) 0600 UTC 10 July 2015.

weight function peaks at around 400, 600, and 800 hPa. Channels 1 and 2 are sensitive to the surface and are excluded due to the large surface emissivity error. Only MWHS observations over clear-sky regions are considered. A radiance observation is rejected if the bias-corrected observation minus simulated brightness temperature from model background exceeds either 15 K or three times the specified observation error for brightness temperature. Radiance data from a mixture of surface types (e.g., over coastal areas) or with large

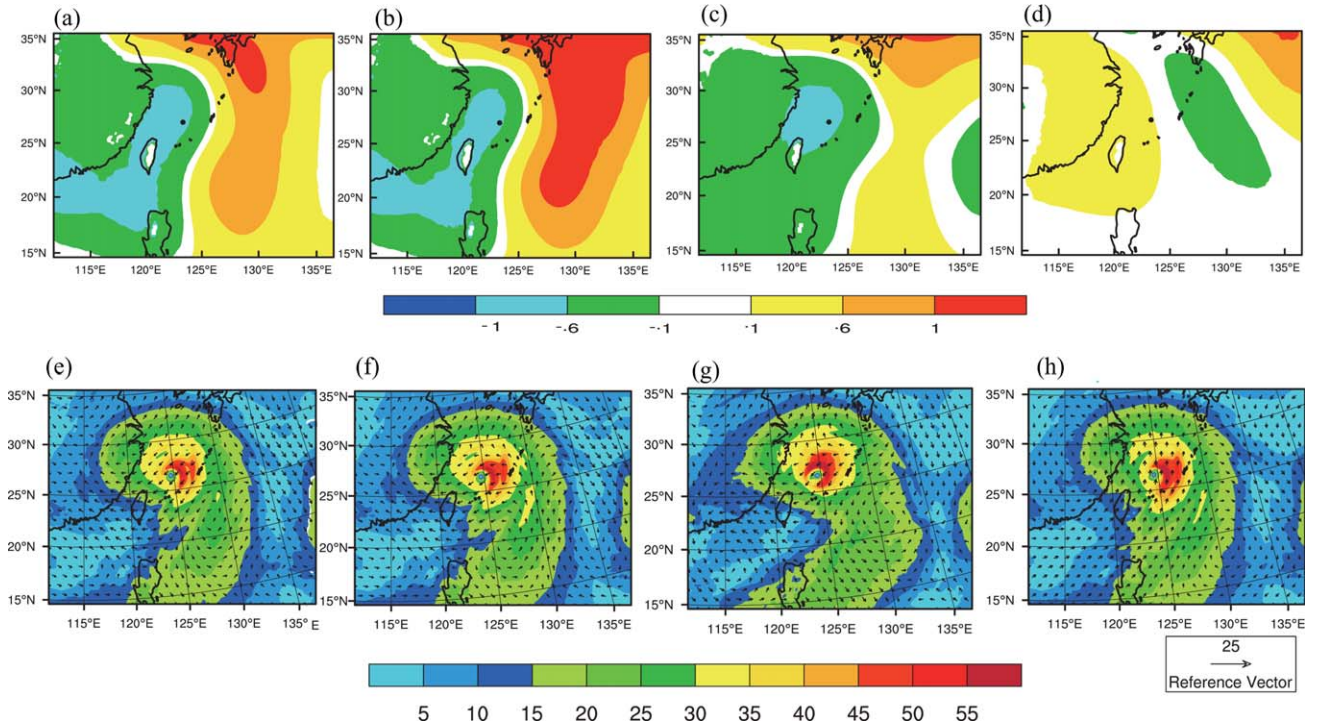

Figure 4. The (a–d) 850 hPa temperature analysis increments and (e–h) 700 hPa wind analysis increments (vectors) and the analyzed wind (shaded) for the (a, e) CTRL-3DVar (b, f) MWHS-3DVar, (c, g) CTRL-Hybrid, and (d, h) MWHS-Hybrid experiments valid at 0600 UTC on 10 July 2015. The typhoon center is denoted as the black dot in Figures 4a–4c.

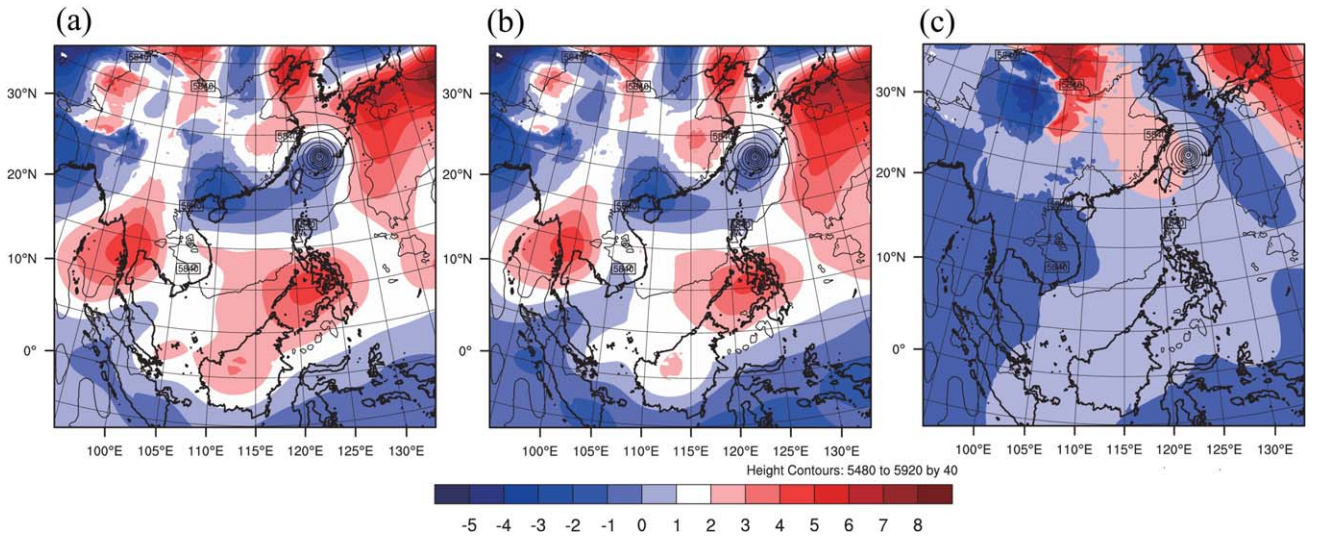

Figure 5. The 500 hPa geopotential height increments (shading) by the (a) CTRL-3DVar, (b) MWHS-3DVar, and (c) MWHS-Hybrid experiments, valid at 0600 UTC on 10 July 2015. The black contours are the 500 hPa geopotential height (m) of the background forecasts.

scan angles on the edge are rejected. MWHS radiance data are thinned using a 90 km grid mesh. Observation data within ± 2 h of the analysis time are selected and assumed to be valid at the analysis time. The MWHS observations available at 0600 UTC on 10 July 2015 and 0600 UTC on 8 July 2015 are shown in Figure 1. Within WRFDA, simulated MWHS brightness temperatures $H(\mathbf{x})$ are calculated with CRTM from temperature and moisture profiles to assimilate high quality radiance data. MWHS is primarily sensitive to water vapor, but in drier atmosphere, it is also sensitive to temperature [*Chouinard and Hallé*, 2003].

The WRF model [*Skamarock et al*., 2008] is employed to forecast with the following physical schemes: The Single-Moment 6-Class scheme [*Hong et al*., 2004]; the Rapid Radiative Transfer Model (RRTM) longwave radiation scheme [*Mlawer et al*., 1997] and the Goddard shortwave [*Chou and Suarez*, 1994]; the Yonsei University (YSU) boundary layer scheme [*Hong et al*., 2006]; the new Kain-Fritsch cumulus parameterization [*Kain and Fritsch*, 1990]; and the Noah land surface model [*Chen and Dudhia*, 2001].

5. Results

The skills of providing the estimation of the true atmospheric state by the CTRL-3DVar, MWHS-3DVar, CTRL-Hybrid, and MWHS-Hybrid experiments are evaluated to consider the impact of the MWHS radiance data, using the different DA methods. The forecasts of wind, temperature, and humidity are compared to the forecasts from conventional observations. The ERA-Interim ($\sim$15 km) reanalysis from the ECMWF [*Chen et al*., 2014] is used in this study for verification, since the ECMWF is considered one of the best centers. The "best track," minimum and sea level pressure data for Chan-hom and Linfa are from the China Meteorological Administration (CMA). The rainfall forecasts are compared to the Tropical Rainfall Measuring Mission (TRMM) [*Gopalan et al*., 2010] rainfall observations.

5.1. Impacts of the MWHS Data on Analyses

5.1.1. Background and 3DVAR Analyses

Figures 2a and 2c show the observed and CRTM-calculated brightness temperature (Tb) from the background for the channel 5 (wavelength: around 13.774 μm) of FY-3B MWHS, while Figures 2b and 2d for the observed and CRTM-calculated brightness temperature (Tb) from the analyses for 0600 UTC 8 July and 0600UTC 10 July using the 3DVAR method. There are significant warm biases in the CRTM-calculated brightness temperatures (Tbs) from the background data, in comparison with the observations (Figures 2a and 2c); this indicates both radiative impacts from the residual cloudy radiance after QC and the erroneous background. More effective QC procedures or cloudy radiance assimilation methods are of potential exploration and improvement. Through minimizing the cost function variationally, the analysis corrects the warm bias (simulated Tb $-$ observed Tb) to a large extent, producing reduced means, standard deviations, and

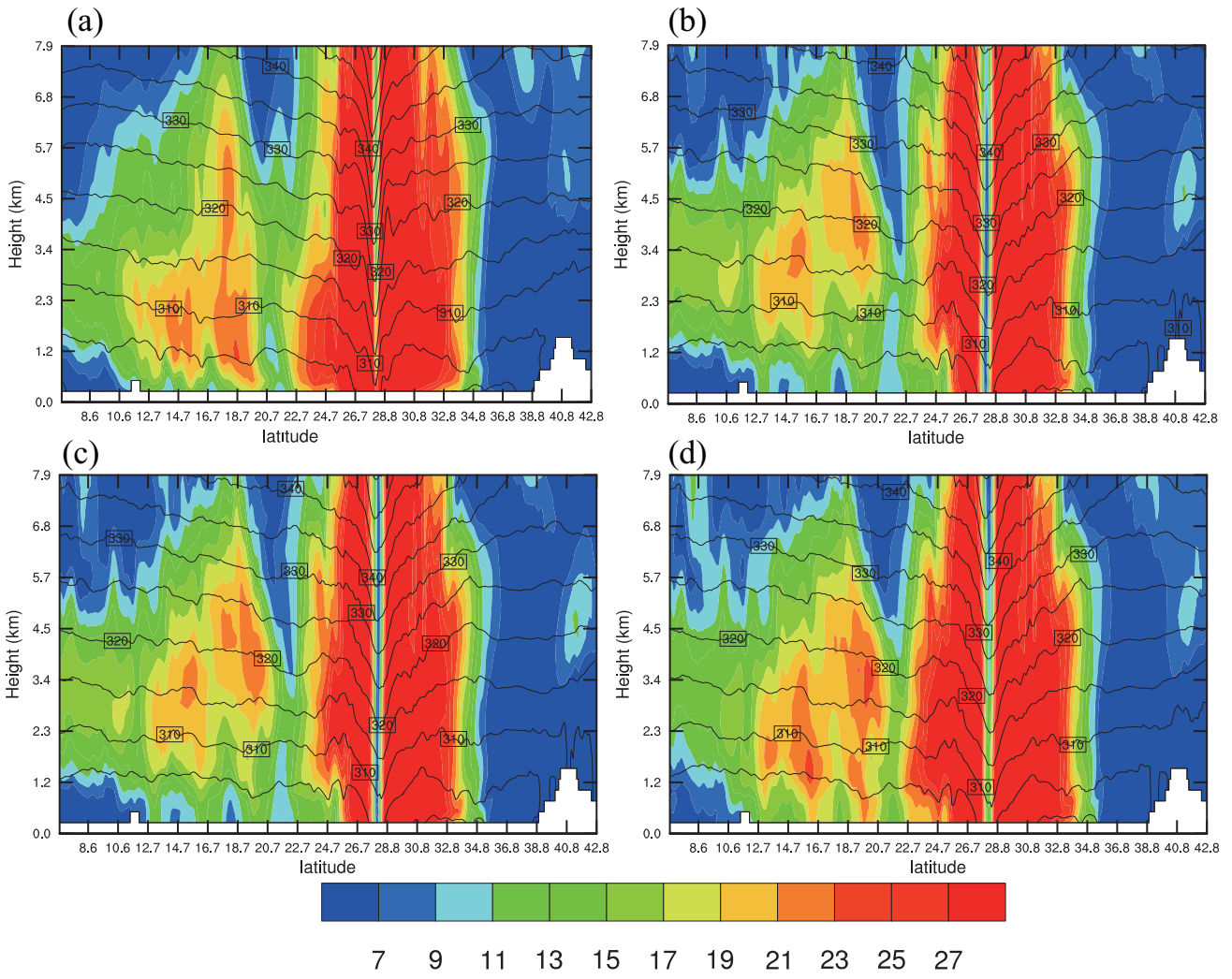

Figure 6. Analyzed horizontal wind speed (shaded) and potential temperature (contours; intervals of 5 K) in south-north vertical cross sections through the analyzed center of Chan-hom for (a) ECMWF ERA-Interim reanalysis, (b) CTRL-3DVar, (c) MWHS-3DVar, and (d) MWHS-Hybrid experiments, at 0600 UTC on 10 July 2015.

root mean square errors in Figures 2b and 2d. The fit between the 3DVAR analysis data and the observations preliminarily validates that the preprocessing and quality control procedures for the raw observations, and the basic DA framework, are overall reliable and efficient.

5.1.2. Ensemble Analyses

The ensemble is the key component in the Hybrid DA procedure, in which an ensemble of models is used to estimate the flow-dependent forecast error. That is, the ensemble-based BEC is incorporated in the Hybrid DA system through a short-term ensemble forecast to allow the model error grow flow-dependently with the weather conditions. The ensemble spread reveals the features of the meteorological conditions and observation locations that constrain the model. The ensemble spreads of wind speed on the 7th model level at the formation of Linfa and Chan-hom (Figure 3), are larger around the typhoons than the surrounding environment, due to the uncertainty of TC predictions. There is also a large spread on the left side of the model domain, because there are few observational data available in western China. The ensemble spread in Figure 3a is applied as the source of the flow-dependent BEC for Linfa. There is also large ensemble spread around 20°N, 133°E, due to the existence of Chan-hom. It is expected that, for Linfa, it will be more appropriate to apply the ensemble-based Hybrid method, to provide a more descriptive in situ BEC matrix.

5.1.3. Analysis Increments

To identify the possible contributions of the DA to create a better TC forecast, the analysis increments for the CTRL-3DVar and MWHS-3DVar experiments are shown in Figures 4a and 4b, where the MWHS radiances

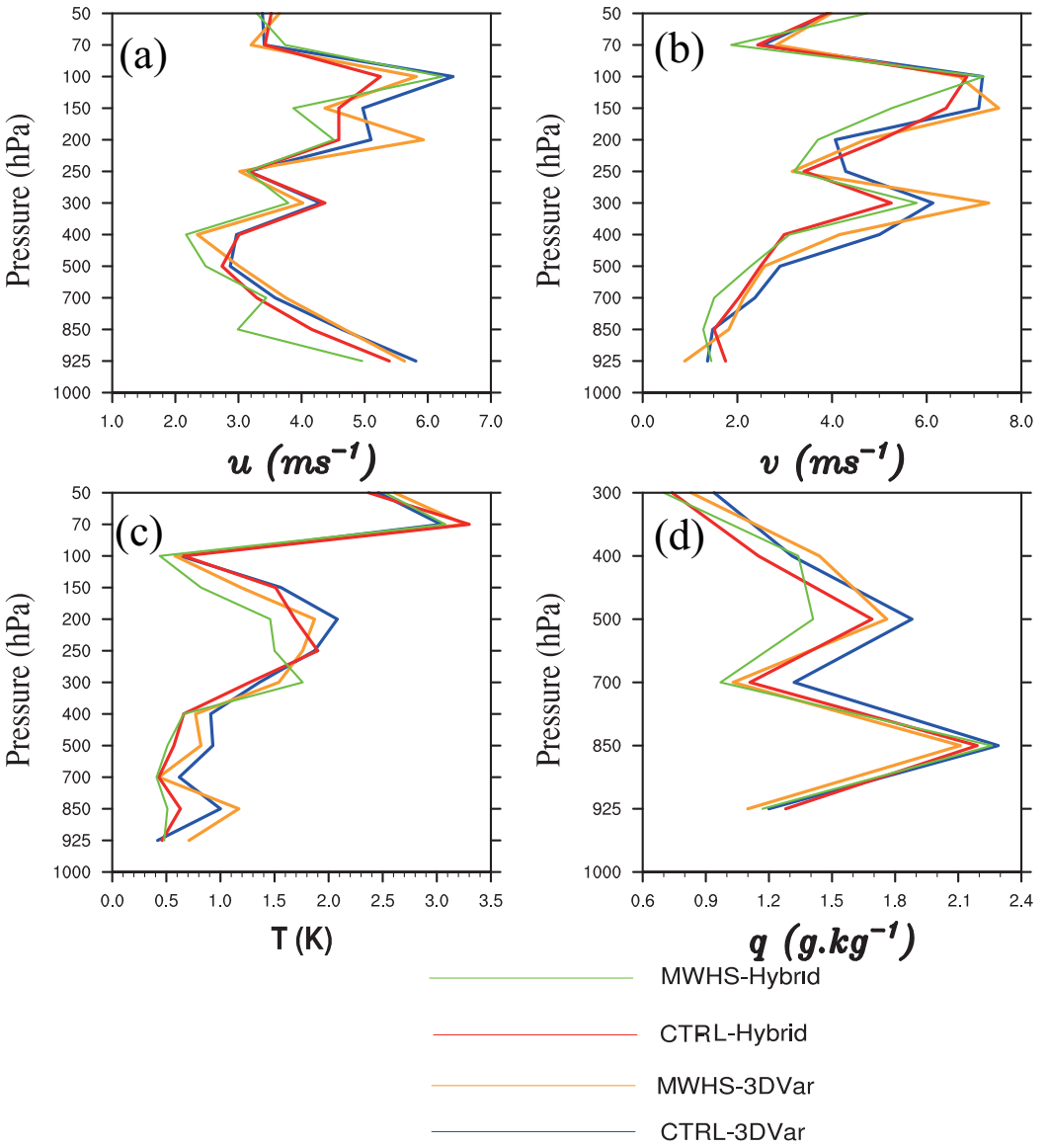

Figure 7. Vertical profiles of 24 h forecast RMSE versus conventional observations for (a) u-wind, (b) v-wind, (c), temperature, and (d) specific humidity (MWHS-Hybrid, green; CTRL-Hybrid, red; MWHS-3DVar, orange; CTRL-3DVar, blue) averaged over the assimilation cycles for Chan-hom and Linfa.

are excluded in the CTRL-3DVar. Figures 4c and 4d show the analysis increments for the CTRL-Hybrid and MWHS-Hybrid experiments, to gain more insight on the DA of radiance data using the static and flow-dependent BECs. In this study, the temperature increments are calculated through multivariate correlations, mainly with the humidity data, since the MWHS observations are assimilated. Using 3DVAR, a cold tongue extends toward the observed typhoon center of Chan-hom (Figures 4a and 4b), and the magnitude is largest near the typhoon center, with positive temperature increments at the east of the typhoon center. The negative temperature increments at lower levels, shown in the MWHS-3DVar experiment, are also found in other simulated typhoon or hurricane centers [*Xiao et al*., 2009; *Shen and Min*, 2015]. By assimilating the MWHS radiance data using 3DVAR, the negative temperature increment is smaller in Figure 4b. Physically, the temperature increments using 3DVAR are not expected to occur inside a typhoon structure, since warming of the vortex inner-core region is supposed to match the enhanced typhoon vortex circulation. As a benefit of the cross variable covariance when assimilating MWHS radiances, a reasonable temperature increment is illustrated by the MWHS-Hybrid experiment (Figure 4d), with the largest magnitudes around the typhoon; this is consistent with the ensemble spread in Figure 3. The positive temperature increments

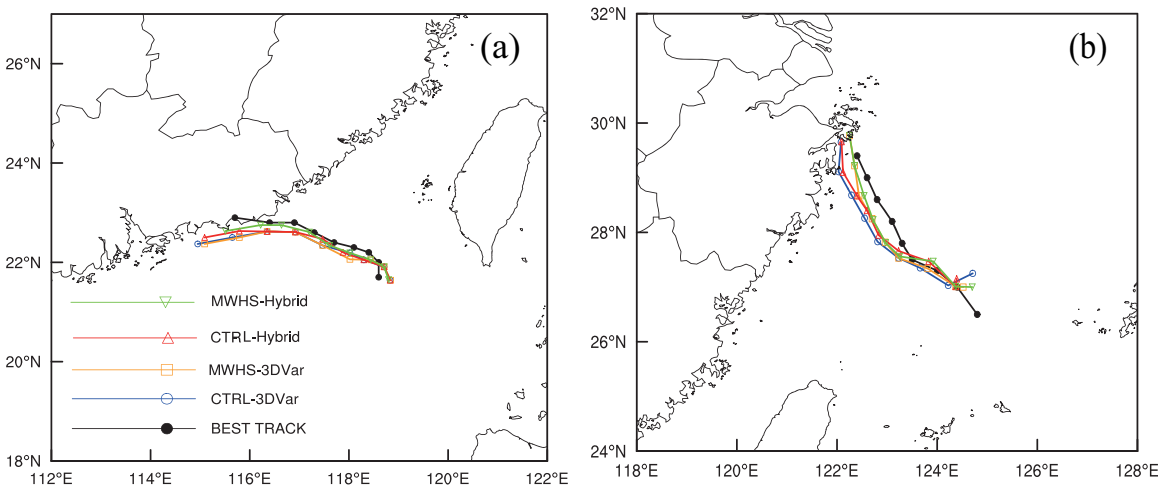

Figure 8. Twenty-four hour track forecasts initialized at (a) 0600 UTC 8 July, 2015, and (b) 0600 UTC 10 July 2015, respectively (best track from the Chinese Meteorological Administration, black; MWHS-Hybrid, green; CTRL-Hybrid, red; MWHS-3DVar, orange; CTRL-3DVar, blue).

at the observed typhoon center are favorable for warm core formations in the typhoon. In addition, using 3DVAR, the limited vertical spatial correlation, due to the use of static BEC, is another factor that produces the negative temperature increments.

For the CTRL-3DVar experiment, the wind vector increments show a clear anticyclonic circulation in the northwest of the observed typhoon center and a southwestward wind around the center (Figure 4e). CTRL-Hybrid experiment does not change the wind field around the vortex center significantly without MWHS radiances. Note that MWHS-3DVar experiment corrects the southwestward wind to be westward. While in the MWHS-Hybrid experiment, a cyclonic wind is found in the west of the observed typhoon center, with clear northward wind increments around the center. These wind increments are consistent with the track forecasts (see section 5.3). It should also be noted that the wind speed magnitude in the analysis is more intense when using the flow-dependent ensemble BEC, reflecting the contribution from the spatially inhomogeneous flow-dependent ensemble BEC (Figures 4e–4h).

Figure 5 shows an example of the 500 hPa geopotential height increments and the geopotential heights of the background data, at 0600 UTC on 10 July 2015. The increments of the CTRL-3DVar and MWHS-3DVar experiments are similar in Figures 5a and 5b. For the CTRL-3DVar experiment, the increments for the surrounding

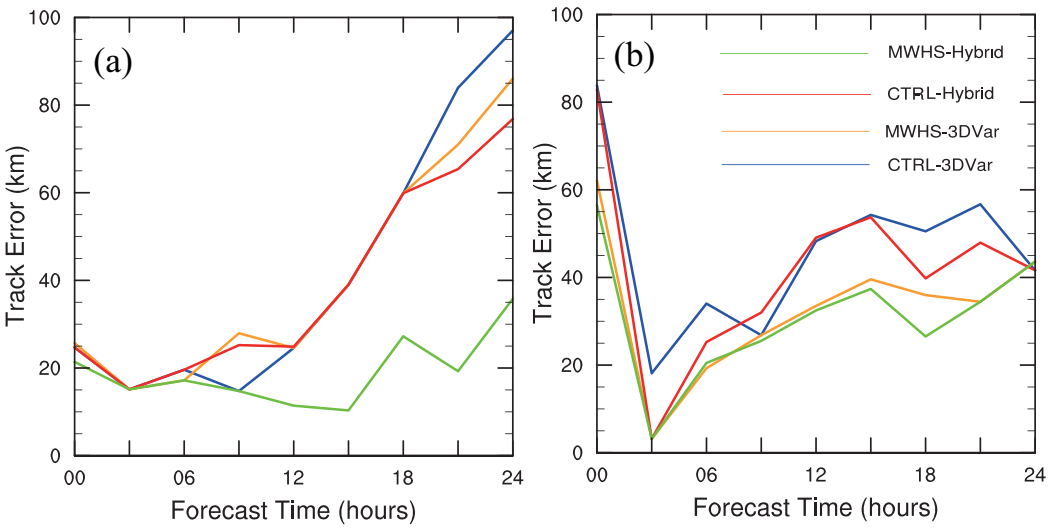

Figure 9. Absolute track forecast errors by lead time, initialized at (a) 0600 UTC 8 July, 2015, and (b) 0600 UTC 10 July, 2015, respectively, for the CTRL-3DVar (blue), MWHS-3DVar (orange), CTRL-Hybrid (red), and MWHS-Hybrid (green) experiments.

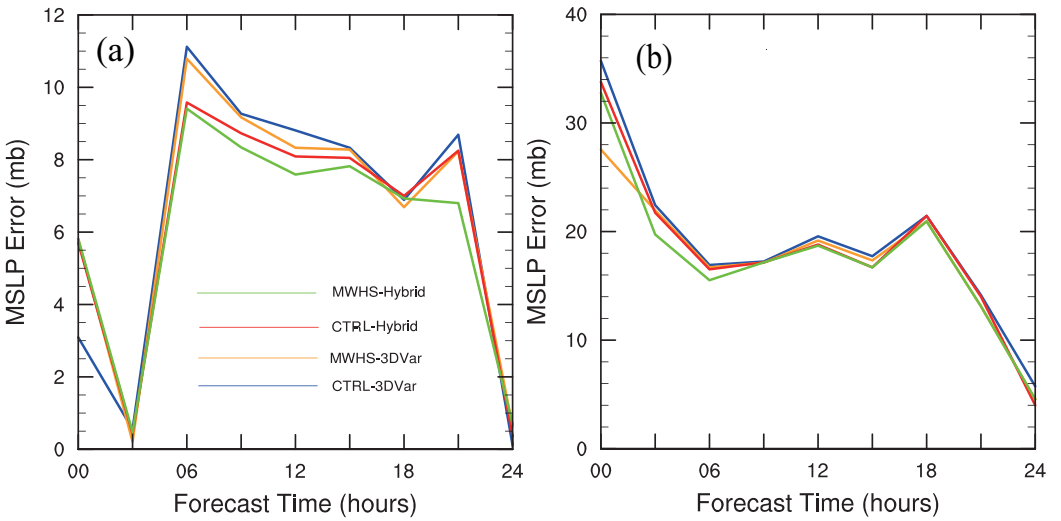

Figure 10. Minimum sea level pressure forecast errors by lead time, initialized at (a) 0600 UTC 8 July 2015, and (b) 0600 UTC 10 July 2015, respectively, for the CTRL-3DVar (blue), MWHS-3DVar (orange), CTRL-Hybrid (red), and MWHS-Hybrid (green) experiments.

environment feature a decrease in height in the southwest of the typhoon, and an increase in the height in the northeast (Figure 5a). By including the MWHS radiance data in the MWHS-3DVar experiment, an obvious height increase is observed in the west of the typhoon center (Figure 5b). Note that here the Hybrid experiment is capable of providing a typhoon-specific BEC matrix shown in Figure 3b. This flow-dependent background error results in much more realistic analysis increments when assimilating conventional and MWHS radiance observations. As shown in Figure 5c, the MWHS-Hybrid experiment increments are quite different for both the typhoon and its surrounding environment, in comparison with the other two 3DVAR experiments (i.e., CTRL-3Dvar and MWHS-3DVar). There is a dipole pattern in the increments of the MWHS-Hybrid experiment, which suggests that the MWHS-Hybrid experiment corrects the position of Chan-hom with the DA procedure by moving the forecasted position to the west, using the flow-dependent ensemble covariance naturally and systematically. The height increments are consistent with the track forecast results (see section 5.3).

5.1.4. Vertical Structures

The impacts of the MWHS data on the analyzed typhoon vertical structure are explored. Figure 6 shows the south-north vertical cross sections of the horizontal wind speed fields and potential temperature, through the analyzed center of Chan-hom, at 0600 UTC on 10July 2015. The wind speed field in the MWHS-3DVar experiment shows tighter circulation patterns than that in the CTRL-3DVar experiment, with an increase of the wind speed on the southern side (Figures 6b and 6c). Figure 6d shows that the MWHS-Hybrid experiment results in a more upright eyewall, to a much higher level than in the MWHS-3DVar experiment. Overall the MWHS-Hybrid experiment (Figure 6d) is most consistent with the ECMWF ERA-Interim (∼15 km) reanalysis (Figure 6a). Meanwhile, there is a presence of a trough located around the typhoon center in the potential temperature fields of the typhoon structure in all experiments. That is, including the MWHS radiance in both the 3DVAR and Hybrid experiments shows less obvious improvement for the potential temperature field than for the winds, which is consistent with *Liu et al*. [2012] and *McNally* [2007].

5.2. Forecast Verification Against Conventional Data

Figure 7 displays vertical profiles of the 24 h forecast root mean square error (RMSE) for u-wind, w-wind, temperature, and specific humidity averaged over the assimilation cycles for Chan-hom and Linfa. The assimilation of MWHS data using 3DVAR does not improve the wind forecasts significantly (Figures 7a and 7b). For temperature, the MWHS-3DVar experiment outperforms the CTRL-3DVar experiment at most pressure levels (Figure 7c), because the observation operator for MWHS sensor is sensitive to both temperature and moisture. There are also clear, positive impacts of MWHS assimilation on the forecasts of specific humidity at levels higher than 850 hPa (Figure 7d). At almost all levels, the MWHS-Hybrid experiment agrees best with the observations for all variables, compared to the other two experiments, especially for specific humidity. CTRL-Hybrid is slightly worse than MWHS-Hybrid. The impact of incorporating the MWHS radiance

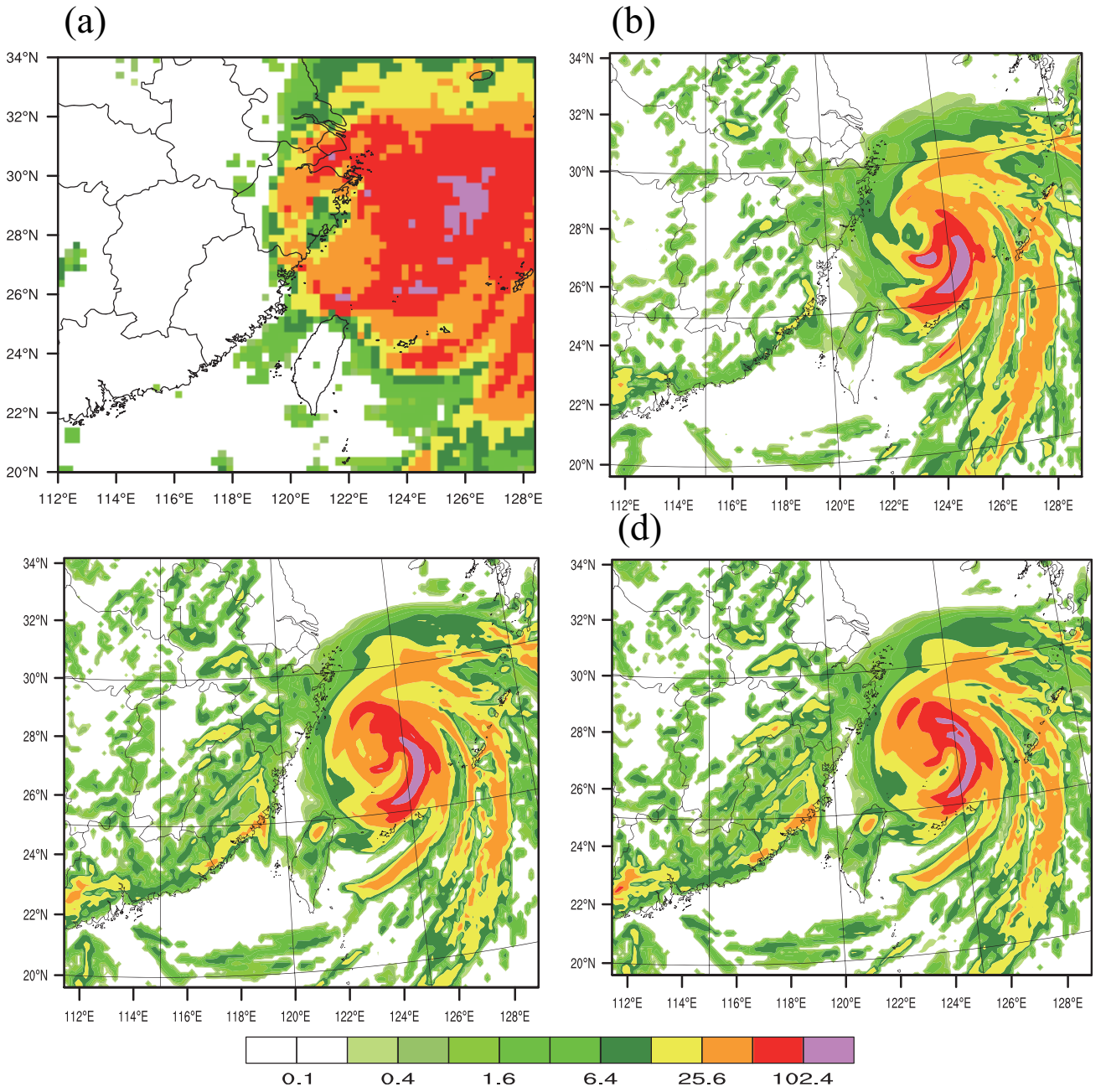

Figure 11. The 24 h accumulated precipitation (mm) according to the (a) TRMM observations, (b) CTRL-3DVar, (c) MWHS-3DVar, and (d) MWHS-Hybrid experiments, initialized at 0600 UTC on 10 July 2015.

data (humidity sensitive channels) on the forecasts of wind and temperature likely result from the use of multivariate correlations, as implied in the WRF Hybrid BEC. *Zou et al.* [2013] and *Newman et al.* [2015] described decreases in forecast skill associated with the assimilation of MHS data and attributed these to the less rigorous QC algorithm in both GSI and WRFDA system, which is mostly based on the innovation check [*Yan et al.*, 2010; *Zou et al.*, 2013]. This study provides further evidence for implementing enhanced QC procedures, when assimilating MWHS radiance data, which was introduced in section 4.

5.3. Track and Intensity Forecast Verification

To demonstrate the impact of DA on the TC forecasts, the 24 h track forecasts of Linfa, initialized at 0600 UTC 8 July 2015, are shown in Figure 8a; the best track from the CMA is used as a reference. The forecast

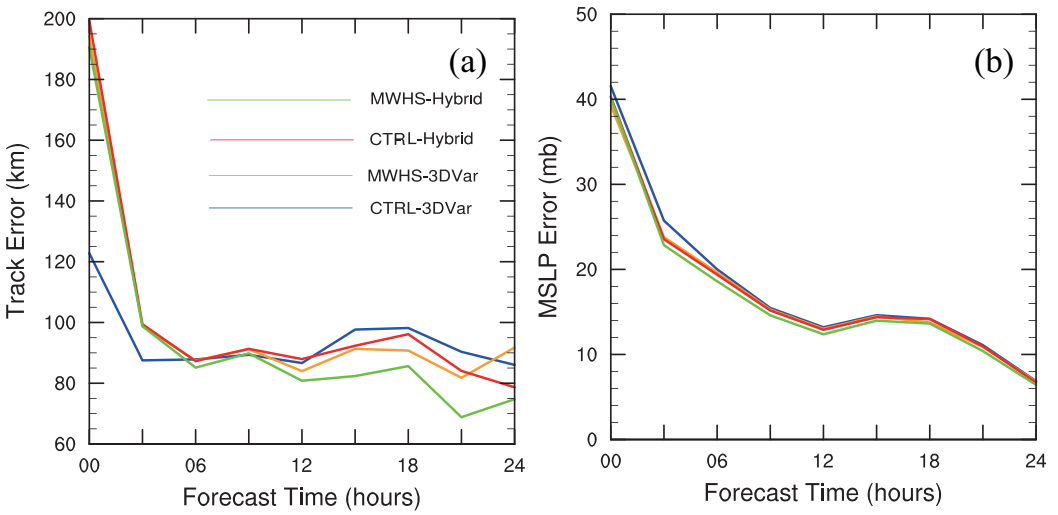

Figure 12. (a) Mean track error and (b) minimum sea level pressure forecast errors by lead time for the CTRL-3DVar (blue), MWHS-3DVar (orange), CTRL-Hybrid (red), and MWHS-Hybrid (green) experiments.

track in the MWHS-Hybrid experiment fits most closely to the CMA track. The southward biases from the tracks that the CTRL-3DVar, MWHS-3DVar, and CTRL-Hybrid experiments produce are all significant. CTRL-Hybrid slightly prevents the southward track bias compared to CTRL-3DVar, MWHS-3DVar. The track from the CTRL-3DVar is moving too fast. The MWHS-Hybrid produces the track forecast fitting the best track most closely, by assimilating the MWHS radiance data with the Hybrid method.

The 24 h track forecasts of Chan-hom in Figure 8b (initialized at 0600 UTC 10July 2015) show that the forecast tracks from experiments using MWHS data with either 3DVAR or Hybrid method agree much better with the CMA track than those the experiments without MWHS radiances produce, which is consistent with the northeastward wind increments in Figure 4d. The improvement in assimilating the MWHS radiance data using the Hybrid method compared to using 3DVAR method is slight. MWHS-Hybrid corrects the south bias from the CTRL-3DVar experiment, which can be attributed to the reasonable height increments in Figure 5c. It is noted that, for Linfa, it is more appreciable for the Hybrid experiment to provide a suitable BEC matrix for DA, due to the coexistence of Chan-hom, than using 3DVAR.

Figure 9 displays the mean absolute track errors for Linfa and Chan-hom that each experiment produces. For Linfa (Figure 9a), the track errors for the CTRL-3DVar and MWHS-3DVar experiments are close. The track errors favor the MWHS-3DVar experiment after an 18 h forecast lead-time for Linfa (Figure 9a). The reductions of the absolute track errors reach 40 km in the MWHS-Hybrid experiment, before Linfa makes landfall. For Chan-hom, the improvements for the track forecasts are generally obvious in both the MWHS-3DVar and MWHS-Hybrid (∼20 km) experiments. Generally, using MWHS radiance data with the Hybrid method produces best track forecasts, while without MWHS radiances with the 3DVAR method produce largest track errors.

The minimum sea level pressure (MSLP) errors as a function of forecast range for Linfa and Chan-hom show the CTRL-3DVar experiment to be better for the first 3 h (Figure 10a). The MWHS-3DVar experiment, with MWHS radiance data, improves the MSLP error slightly for the remainder of the time, by ∼1 mb error. The MWHS-Hybrid experiment further positively impacts the MSLP for the last 21 h. Consistent improvement (∼1 mb) in the forecast of MSLP is achieved for Chan-hom, starting from the analysis time to the 24 h forecast lead time by both the MWHS-3DVar and MWHS-Hybrid experiments, compared to the CTRL-3DVar and CTRL-Hybrid experiments (without MWHS radiances) (Figure 10b).

5.4. Precipitation Forecast Verification

Accurate prediction of precipitation both near and after landfall of typhoons or hurricanes are very important for warnings of inland floods; Figure 11 shows the total accumulated precipitation fields during the 24 h forecast period from the CTRL, MWHS-3DVar, and MWHS-Hybrid experiments, in comparison with the TRMM rainfall observations. The observed precipitation shows a maximum spiral band pattern near (29°N, 126°E) and a band of heavy precipitation along the coast of Zhejiang

Province. It is obvious that the CTRL experiment forecasts the precipitation pattern slightly southward; this may be due to its southward track bias and low intensity. In addition, the CTRL significantly underestimates the accumulated precipitation over land. Note that the southward bias in the precipitation location is mitigated and the accumulated precipitation is increased over land in the MWHS-3DVar experiment. However, compared with the CTRL and MWHS-3DVar experiment, the MWHS DA experiment using the Hybrid method shows significant improvements (Figure 11d). MWHS-Hybrid corrects the precipitation location northward and the amount of precipitation it reproduces is most similar to the observations; this can be attributed to the improvement in the internal structure and track of the typhoon, and its surrounding environment. Despite the encouraging results regarding the TC precipitation forecast, the errors remain large, due to the limitations of dynamics and physical parameterizations in WRF.

5.5. Statistical Results Over Six Cases

Statistical results based on multiple binary typhoon cases are provided to further validate the robustness of the results from Chan-hom and Linfa. This section selects four binary typhoons, Fitow and Danas in 2013 and Matmo and Rammasun in 2014 as new cases. Among them, Fitow in 2013, Matmo in 2014, and Rammasun in 2014 made landfall over east coast of China. Similar data assimilation experiments are conducted following those for Chan-hom and Linfa.

The mean track errors and MSLP errors averaged over the six typhoons are shown in Figure 12a. Overall, the track errors for the experiments with MWHS (MWHS-3DVar and MWHS-Hybrid) are smaller than those for the CTRL-3DVar and CTRL-Hybrid experiments. By using the Hybrid method, improvements for the track forecasts are obvious, especially for the MWHS-Hybrid experiments. For the MSLP errors, MWHS-Hybrid outperforms other experiments slightly for most hours, while other experiments produce very close results.

6. Summary and Future Perspectives

In this study, the impact of the FY-3B MWHSs radiance data on the analyses and forecasts of the binary Linfa and Chan-hom typhoons are assessed, using the regional WRF model and its 3DVAR and Hybrid DA systems. Assimilating MWHS radiance using 3DVAR slightly improves the descriptive wind and temperature fields in the WRF model and obviously improves the humidity forecasts, at levels higher than 850 hPa; the use of 3DVAR yields better track, intensity, and precipitation forecasts, compared to the CTRL experiment, without MWHS DA. The Hybrid experiment further improves the track, intensity, and rainfall forecasts. With the Hybrid method, the water vapor information from MWHS better supplies mesoscale information, through the multivariable correlation with the flow-dependent background error. For Linfa, with the coexistence of Chan-hom, it is more appreciable for the Hybrid method (ensemble/3DVAR) to provide a more descriptive BEC matrix than using 3DVAR alone. Experiments on multiple binary typhoon cases are also provided, which further validated the robustness of the results on the FY-3B satellite MWHS radiance data assimilation.

There are some areas for further explorations and improvements; the refinement of the assumed observation errors and QC schemes of the data could potentially increase the impact of the MWHS data. More MWHS radiance channels should be explored, using an effective surface emissivity-modeling scheme. The combination of the Ensemble/3DVAR Hybrid DA [*Wang et al*., 2008; *Schwartz et al*., 2013] and four-dimensional variational (4DVAR) [*Huang et al*., 2009] methods is also planned, to better utilize more radiance data and other in situ observations, in a flow-dependent manner, at appropriate times.

Acknowledgments

This work was jointly sponsored by the 973 Program (grant 2013CB430102), the Beijige Funding from Jiangsu Research Institute of Meteorological Science (BJG201510), the National Natural Science Foundation of China (41375025), and the Priority Academic Program Development of Jiangsu Higher Education Institutions (PAPD). The FY radiance data were obtained freely from (http://fy3.satellite.cma.gov.cn). The ECMWF reanalysis data can be downloaded from (http://rda.ucar.edu/datasets/ds113.0/). The author would like to thank the two reviewers for their insightful comments and suggestions that have contributed to improve this paper.

References

Auligné, T., A. P. Dee, and D. P. McNally (2007), Adaptive bias correction for satellite data in a numerical weather prediction system, *Q. J. R. Meteorol. Soc.*, *133*, 631–642.

Barker, D., et al. (2012), The weather research and forecasting (WRF) model's community variational/ensemble data assimilation system: WRFDA, *Bull. Am. Meteorol. Soc.*, *93*, 831–843.

Chen, F., and J. Dudhia (2001), Coupling an advanced land-surface/hydrology model with the Penn State/NCAR MM5 modeling system. Part I: Model description and implementation, *Mon. Weather Rev.*, *129*, 569–585.

Chen, G., T. Iwasaki, H. Qin, and W. Sha (2014), Evaluation of the warm-season diurnal variability over East Asia in recent reanalyses JRA-55, ERA-Interim, NCEP CFSR, and NASA MERRA, *J. Clim.*, *27*(14), 5517–5537.

Chen, K., S. English, N. Bormann, and J. Zhu (2015), Assessment of FY-3A and FY-3B MWHS Observations, *Weather Forecasting*, *30*, 1280–1290.

Chou, M. D., and M. J. Suarez (1994), An efficient thermal infrared radiation parameterization for use in general circulation models, NASA Technical Memorandum, National Aeronautics and Space Administration, Md.
Chouinard, C., and J. Hallé (2003), The assimilation of AMSU-B radiances in the CMC global data assimilation system: Difficulties and impact relative to AMSU-A radiances, paper presented at the TOVS Study Conference, Sainte Adele, Canada.
Collard, A., J. Derber, R. Treadon, N. Atkinson, J. Jung, and K. Garrett (2012), Toward assimilation of CrIS and ATMS in the NCEP Global Model, paper presented at the 18th International TOVS Study Conference, International Atovs working group, Toulouse, France.
Dee, D. P., and S. M. Uppala (2009), Variational bias correction of satellite radiance data in the ERA-Interim reanalysis, *Q. J. R. Meteorol. Soc.*, *135*, 1835–1841.
Derber, J. C., and W. S. Wu (1998), The use of TOVS clear-sky radiances in the NCEP SSI analysis system. *Mon. Weather Rev.*, *126*, 2287–2299.
Dong, P., J. Huang, X.-Y. Huang, Z. Liu, and X. Zhang (2013) Implement and preliminary experiment of FY-3 and NPP microwave satellite data assimilation, paper presented at WRFDA 14th Annual WRF User's Workshop, Nat. Cent. Atmos. Res., Boulder, Colo.
Eyre, J. R. (1992), *A Bias Correction Scheme for Simulated TOVS Brightness Temperatures*, ECMWF, Reading, U.K.
Goodrum, G., K. B. Kidwell, and W. Winston, Eds. (1999), *NOAA KLM User's Guide. National Oceanic and Atmospheric Administration*, Md., [CD-ROM].
Gopalan, K., N.-Y. Wang, R. Ferraro, and C. Liu (2010), Status of the TRMM 2A12 land precipitation algorithm, *J. Atmos. Oceanic Technol.*, *27*, 1343–1354.
Guan, L., X. Zou, F. Weng, and G. Li (2011), Assessments of FY-3A microwave humidity sounder measurements using NOAA-18 microwave humidity sounder, *J. Geophys. Res.*, *116*, D10106, doi:10.1029/2010JD015412.
Han, Y., P. van Delst, Q. Liu, F. Weng, B. Yan, R. Treadon, and J. Derber (2006), JCSDA Community Radiative Transfer Model (CRTM)—Version 1, *NOAA Tech. Rep. 122*, 33 pp., NESDIS, Md.
Harris, B. A., and G. Kelly (2001), A satellite radiance-bias correction scheme for data assimilation, *Q. J. R. Meteorol. Soc.*, *127*, 1453–1468.
Holloway, C. E., and J. D. Neelin (2009), Moisture Vertical Structure, Column Water Vapor, and Tropical Deep Convection, *J. Atmos. Sci.*, *66*, 1665–1683.
Hong, S.-Y., J. Dudhia, and S.-H. Chen (2004), A revised approach to ice microphysical processes for the bulk parameterization of clouds and precipitation, *Mon. Weather Rev.*, *132*, 103–120.
Hong, S.-Y., Y. Noh, and J. Dudhia (2006), A new vertical diffusion package with an explicit treatment of entrainment processes, *Mon. Weather Rev.*, *134*, 2318–2341.
Huang, X.-Y., et al. (2009), Four-dimensional variational data assimilation for WRF: Formulation and preliminary results, *Mon. Weather Rev.*, *137*, 299–314.
Ide, K., P. Courtier, M. Ghil, and A. C. Lorenc (1997), Unified notation for data assimilation: Operational, sequential and variational, *J. Meteorol. Soc. Jpn.*, *75*, 181–189.
Kain, J. S., and J. M. Fritsch (1990), A one-dimensional entraining/detraining plume model and its application in convective parameterization, *J. Atmos. Sci.*, *47*, 2784–2802.
Li, J., and H. Liu (2009), Improved hurricane track and intensity forecast using single field-of-view advanced IR sounding measurements, *Geophys. Res. Lett.*, *36*, L11813, doi:10.1029/2009GL038285.
Liu, Q., and F. Weng (2006), Advanced doubling-adding method for radiative transfer in planetary atmosphere, *J. Atmos. Sci.*, *63*, 3459–3465.
Liu, Z., C. S. Schwartz, C. Snyder, and S.-Y. Ha (2012), Impact of assimilating AMSU-A radiances on forecasts of 2008 Atlantic tropical cyclones initialized with a limited-area ensemble Kalman filter, *Mon. Weather Rev.*, *140*, 4017–4034.
Lorenc, A. C. (1986), Analysis methods for numerical weather prediction, *Q. J. R. Meteorol. Soc.*, *112*, 1177–1194.
Lu, Q. F. (2011a), Initial evaluation and assimilation of FY-3A atmospheric sounding data in the ECMWF System, *Sci. China Earth Sci.*, *54*, 1453–1457.
Lu, Q. F., W. Bell, P. Bauer, N. Bormann, and C. Peubey (2011b), Characterizing the FY-3A microwave temperature sounder using the ECMWF model, *J. Atmos. Oceanic Technol.*, *28*, 1373–1389.
McNally, A. P., J. C. Derber, W. Wu, and B. B. Katz (2000), The use of TOVS level-1b radiances in the NCEP SSI analysis system, *Q. J. R. Meteorol. Soc.*, *126*, 689–724.
McNally, T. (2007), The use of satellite data in polar regions, in *ECMWF Seminar Proceedings on Polar Meteorology*, European Centre for Medium-Range Weather Forecasts, Reading, U. K.
Mlawer, E. J., S. J. Taubman, P. D. Brown, M. J. Iacono, and S. A. Clough (1997), Radiative transfer for inhomogeneous atmosphere: RRTM, a validated correlated-k model for the long-wave, *J. Geophys. Res.*, *102*, 16,663–16,682.
Newman, K. M., C. S. Schwartz, Z. Liu, H. Shao, and X.-Y. Huang (2015), Evaluating forecast impact of assimilating microwave humidity sounder (MHS) radiances with a regional ensemble Kalman filter data assimilation system, *Weather Forecasting*, *43*, 964–983.
Niels, B., F. Anne, and B. William (2012), Evaluation and assimilation of ATMS data in the ECMWF system, *Technical Memorandum 689*, 16 pp., ECMWF, European Centre for Medium-Range Weather Forecasts, Reading, U. K.
Parrish, D. F., and J. C. Derber (1992), The National Meteorological Center's spectral statistical-interpolation analysis system, *Mon. Weather Rev.*, *120*, 1747–1763.
Schwartz, C. S., and Z. Liu (2014), Convection-permitting forecasts initialized with continuously cycling limited-area 3DVAR, ensemble Kalman filter, and "Hybrid" variational–ensemble data assimilation systems, *Mon. Weather Rev.*, *142*, 716–738.
Schwartz, C. S., Z. Liu, Y. Chen, and X.-Y. Huang (2012), Impact of assimilating microwave radiances with a limited-area ensemble data assimilation system on forecasts of Typhoon Morakot, *Weather Forecasting*, *27*, 424–437.
Schwartz, C. S., Z. Liu, X.-Y. Huang, and Y.-H. Kuo (2013), Comparing limited-area 3DVAR and Hybrid variational-ensemble data assimilation methods for typhoon track forecasts: Sensitivity to outer loops and vortex relocation, *Mon. Weather Rev.*, *141*, 4350–4372.
Shen, F., and J. Min (2015), Assimilating AMSU-A radiance data with the WRF Hybrid En3DVAR system for track predictions of Typhoon Megi (2010), *Adv. Atmos. Sci.*, *9*, 1231–1243.
Shen, F., J. Min, and D. Xu (2015), Assimilation of Radar radial velocity data with the WRF Hybrid ETKF-3DVAR system for the prediction of Hurricane Ike (2008), *Atmos. Res. 169*, 127–138. doi:10.1016/j.atmosres.2015.09.019.
Skamarock, W., J. B. Klemp, J. Dudhia, D. O. Gill, D. Barker, M. G. Duda, X.-Y. Huang, and W. Wang (2008). A description of the Advanced Research WRF version 3, NCAR Technique Note, National Center for Atmospheric Research, Boulder, Colo.
Smith, W. L., H. M. Woolf, C. M. Hayden, D. Q. Wark, and L. M. McMillin (1979), The TIROS-N operational vertical sounder, *Bull. Am. Meteorol. Soc.*, *60*, 1177–1187.
Thépaut, J.-N. (2003), Satellite data assimilation in numerical weather prediction: An overview, in Proceedings of the Seminar on Recent Developments in Data Assimilation for Atmosphere and Ocean, pp. 75–96, ECMWF, Reading, U.K.

Wang, X. (2011), Application of the WRF Hybrid ETKF-3DVAR data assimilation system for hurricane track forecasts, *Weather Forecasting*, *26*, 868–884.

Wang, X., D. M. Barker, C. Snyder, and T. M. Hamill (2008), A Hybrid ETKF-3DVAR data assimilation scheme for the WRF model, Part I: Observing system simulation experiment, *Mon. Weather Rev.*, *136*, 5116–5131.

Xiao, Q., X. Zhang, C. Davis, J. Tuttle, G. Holland, and P. J. Fitzpatrick, (2009), Experiments of hurricane initialization with airborne Doppler radar data for the Advanced Research Hurricane WRF (AHW) model, *Mon. Weather Rev.*, *137*, 2758–2777.

Xu D., Z. Liu, X.-Y. Huang, J. Min, and H. Wang (2013), Impact of assimilating IASI radiance observations on forecasts of two tropical cyclones, *Meteorol. Atmos. Phys.*, *122*, 1–18.

Xu, D., T. Auligné, and X.-Y. Huang (2015), A retrieval method for 3-D cloud parameters using radiance observations from multiple satellites, *Adv. Atmos. Sci.*, *32*, 349–362.

Yan, B., F. Weng, and J. Derber (2010), Assimilation of satellite microwave water vapor sounding channel data in NCEP Global Forecast System (GFS), paper presented at 17th International TOVS Study Conference, Int. ATOVS Working Group, Monterrey, Calif.

Yen, T.-H., C.-C. Wu, and G.-Y. Lien (2011), Rainfall simulations of Typhoon Morakot with controlled translation speed based on EnKF data assimilation. *Terrestrial, Atmos. Oceanic Sci.*, *22*, 647–660.

Zapotocny, T. H., J. A. Jung, J. F. L. Marshall, and R. E. Treadon (2008), A two-season impact study of four satellite data types and rawinsonde data in the NCEP Global Data Assimilation System, *Weather Forecasting*, *23*, 80–100.

Zou, X., X. Wang, F. Weng, and G. Li (2011). Assessments of Chinese Fengyun Microwave Temperature Sounder (MWTS) measurements for weather and climate applications, *J. Atmos. Oceanic Technol.*, *28*, 1206–1227.

Zou, X., Z. Qin, and F. Weng (2013), Improved quantitative precipitation forecasts by MHS radiance data assimilation with a newly added cloud detection algorithm, *Mon. Weather Rev.*, *141*, 3203–3221.